11th International Symposium on Turbulence and Shear Flow Phenomena (TSFP11)
Southampton, UK, July 30 to August 2, 2019

TURBULENT DRAG REDUCTION IN TAYLOR-COUETTE FLOWS USING SUPER-HYDROPHOBIC SURFACES

Suhail Naim*, **M.F. Baig** †**& Fuaad P.A** ‡
Department of Mechanical Engineering, Z.H. College of Engineering and Technology
Aligarh Muslim University, Aligarh-202002, India
mfbaig.me@amu.ac.in

ABSTRACT

The present work involves study of turbulent drag reduction in an incompressible turbulent Taylor-Couette flow using 'idealized' Super Hydrophobic Surfaces (SHS). Three-dimensional DNS studies using finite difference method in cylindrical annuli have been performed at Reynolds number 4000, aspect ratio($\Gamma = 6.0$), and radius ratio(η)= 0.5 and 0.67 . The SHS comprises of streamwise/azimuthal microgrooves(MG), transverse/longitudinal MG ,spiral MG and microposts MG. The SHS are modelled as shear-free zones. We found drag reduction to be maximum for streamwise SHS grooves. We have tried to understand the role of the effective slip and modifications to the turbulence dynamics responsible for drag reduction using turbulence statistics and turbulence kinetic energy. We found slip to be playing the dominating role in bringing about drag reduction while the turbulence modification was enhancing turbulence kinetic energy. SHS implementation is found to be associated with turbulence enhancement yet we observe drag reduction for almost all the cases, hence slip is the major contributor to drag reduction.

1 Introduction

Modifying the texture and wetting behavior of a surface can have important outcomes for drag reduction. For example, SH surfaces, which includes pockets of air trapped inside micro-scale features on a non-wetting solid surface, have received much attention over the past decade. A SH surface having peaks of microscale protrusions supporting a shear-free air/water interface results in a surface having slip lengths. The concept of slip velocity can be used to define the slip length. The slip velocity U_s is proportional to the shear rate experienced by the fluid at the wall

$$U_s = l_s \left(\frac{\partial u}{\partial r}\right)_{wall} \tag{1}$$

where l_s is the slip length. By averaging over the entire surface,we can obtain an average slip-velocity at the wall, U_s. SHS has been shown to reduce wall shear stress in laminar and turbulent flows by Ou *et al.* (2004), Srinivasan *et al.* (2013), Park *et al.* (2014), Fuaad *et al.* (2016*a*).In such treatments, sustaining drag reduction hinges on the retention of air in the surface features. The air pockets fail when using complex liquids such as crude oil under high pressure and under high shear rates due to dissolution of vapor into the working liquid. Unless the vapor is replenished, for example, by electrolytic methods as shown by Lee & Kim (2011), the drag reducing properties will be lost, and can even result in a drag increase due to roughness effects. Rosenberg *et al.* (2016) achieved drag reduction upto 10 percent by employing streamwise SHS grooves on inner cylinder. Van Buren & Smits (2017) employed transverse SHS grooves on inner cylinder and successfully achieved a drag reduction upto 45 percent. It was found that drag reduction increased with Reynolds number, fluid area fraction, and groove width.
Here, in this study we test different SHS configurations in a turbulent flow on the inner cylinder walls. We perform DNS for a Taylor-Couette flow in the annulus between two concentric cylinders, the outer of which is stationary. This work is being pursued to investigate the mechanism of turbulence mitigation as was observed experimentally by Rosenberg *et al.* (2016) and by Van Buren & Smits (2017) on employing SH grooves in vertical Taylor-couette configuration.

2 Mathematical formulation and numerical scheme

Figure-1 shows the computational domain and the mesh in the $r-\theta$ plane. The numerical simulations are performed using our validated DNS code which employs a finite difference based discretisation on a collocated grid.The non-dimensional governing equations are:

$$\nabla.\mathbf{U} = 0 \tag{2}$$

$$\frac{\partial \mathbf{U}}{\partial t} + \mathbf{U}\cdot\nabla\mathbf{U} = -\nabla\mathbf{P} + \left(1/Re\right)\nabla^2\mathbf{U} \tag{3}$$

The governing equations are subjected to translational-periodicity in azimuthal and axial directions, while no-slip and no-penetration conditions for velocity field apply for inner and outer cylinder walls. There is non-uniform mesh in wall-normal direction while in azimuthal and axial directions it is uniform.
The semi-implicit numerical-scheme employed for DNS simulations of turbulent flows is a modified SMAC scheme originally proposed by Cheng & Armfield (1995) and successfully employed to study turbulent flows by Fuaad *et al.* (2016*a*,*b*); Ahmad *et al.* (2015); Khan &

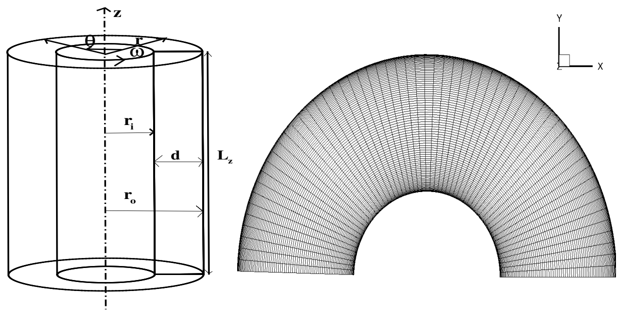

Figure 1. Computational domain with mesh

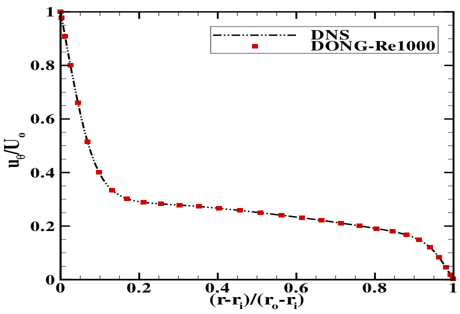

Figure 2. validation results with Dong(2007) at Re 1000

Baig (2016) The Pressure Poisson equation is solved using a SSOR preconditioned GMRES solver in which the error-tolerance of the residual is kept as small as 10^{-5}. A cell-Peclet number (Pe) based hybrid scheme is employed for discretisation of convective terms, using a mix of central and third order upwinding given by Kuwahara (1999). The DNS-code has been extensively validated with the results of Dong (2007) as shown in Figure 2.

Parameter definitions

The geometry of the flow is characterized by the radius ratio, $\eta = r_i/r_o$, where r_i and r_o are the radii of the inner and outer cylinders respectively, and the aspect ratio, $\Gamma = L_z/d = 6.0$ has been taken. Here d is the gap width. The inner cylinder rotates with constant angular velocity Ω, while the outer cylinder is at rest .We have defind the Reynolds number $Re = \frac{U_o d}{\nu}$, where $U_o = \Omega r_i$ is the rotational speed of inner cylinder.

SHS model

Locally along the interface, both external and internal fluids must exhibit the same slip velocity, U_s i.e u_θ, u_z , and shear stress. We can express the second matching condition at the interface, in the following manner

$$N\frac{\partial U_{ext}}{\partial r}|_i = \frac{\partial U_{int}}{\partial r}|_i \tag{4}$$

with the viscosity ratio, N, defined as the ratio of the viscosity of the external fluid, μ_{ext} , to that of the infused liquid, μ_{int} , given by N = μ_{ext} / μ_{int} . Also, $\frac{\partial U}{\partial r}$ is defined as the surface-normal gradient of the azimuthal velocity and axial velocity for the respective fluids. As we decrease the viscosity within the groove, and N gets increased, the gas/fluid interface is able to sustain a higher slip velocity; specifically, in the limit when N tends to infinity, we expect the gas/fluid interface to behave as a shear-free boundary. We have used zero normal velocity at interface to keep it planar for simplification. For air as the trapped fluid, N is around 55, making the derivatives on the inner side tending to zero ; so making the calculations inside the trapped air zone avoidable. The gas/liquid interfaces on SHS have been modelled as idealized flat, shear-free boundaries.

On the shear-free boundaries, normal velocity is kept zero to keep the interface planar. The azimuthal and axial velocities at shear-free boundaries have been computed by setting respective shear stresse $\tau_{r\theta} = \tau_{rz}$ =0. Figure 3 shows the various patterns of SH surfaces. On the top of the ridges no-slip condition has been imposed along with no-peneteration condition.

Table-1 shows the grid spacing employed in streamwise, spanwise and wall-normal directions. Table-2 shows the features width(W) and gap(G) within them of various SHS employed. The ratio of shear free area and total area denoted as 'a' has been kept 0.5 for all cases.

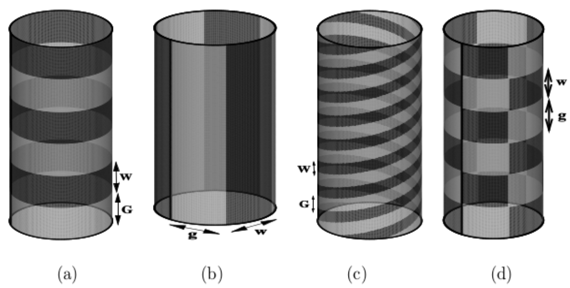

Figure 3. grey portion represents slip and black no-slip of SHS

Table 1. Grid spacings employed

case	Re	Re_τ	η	Γ	Δr^+_{min}	$\Delta r\theta^+$	Δz^+
SHS	4000	256	0.5	6.0	0.06	6.7	6.0
SHS	4000	286	0.67	6.0	0.07	7.48	3.35

Table 2. Features width(W) & gap(G) within them.

case	η	W/d	G/d	W/G	a
4kcg	0.5	1	1	1	0.5
4kag	0.5	$2\pi/6 \sim 1.05$	$2\pi/6 \sim 1.05$	1	0.5
4kposts	0.5	1	1	1	0.5
4ksp	0.5	0.37	0.37	1	0.5
$4k_g$cg	0.67	1	1	1	0.5
$4k_g$ag	0.67	$\sim$2.1	$\sim$2.1	1	0.5
$4k_g$posts	0.67	1	1	1	0.5
$4k_g$sp	0.67	0.37	0.37	1	0.5

3 Results and Discussions

To assess the roles of effective slip on the walls versus modifications to the dynamics of turbulence within the flow, a series of DNS studies were performed in turbulent SH Taylor-Couette flow with various patterns of azimuthal MG, micro-posts, spiral MG and longitudinal MG. We

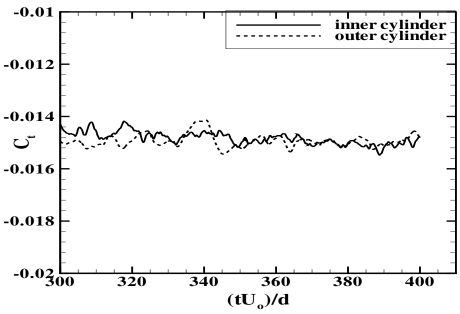

Figure 4. Time history of instantaneous coefficient of torque, at inner(-) & outer(...) cylinder for 4kag case.

Table 3. Mean slip vlocity(u_s), Slip length(λ^+) in viscous units & drag variation in response to different SHS at Re=4000 and $\eta = 0.5$.

Case	Re	$(u_\theta)_s$	$(u_\theta)_s^+$	λ_θ^+	$(u_z)_s$	$(u_z)_s^+$	%DR
4kcg	4000	0.3833	5.99	8.6	0.0146	0.23	31.3
4kag	4000	0.1134	1.77	1.96	0.00466	0.07	10.84
4kposts	4000	0.116	1.81	1.98	0.00212	0.03	9.64
4ksp	4000	0.121	1.89	1.98	0.0023	0.036	7.3
Min & Kim (2004)(a)	4200	-	1.707	1.783	-	1.707	8.00
(b)	4200	-	3.238	3.566	-	3.238	17.00

have also studied the effect of decreasing the gap between the cylinders, thereby decreasing characteristic length gap-width which results in enhanced radius ratio η(0.67 from initial 0.5) while maintaining the same aspect ratio Γ. The percentage change in drag(DR%) has been defined as

$$DR\% = \frac{(\tau_w)_{uc} - (\tau_w)_c}{(\tau_w)_{uc}} * 100 \tag{5}$$

where subscripts 'uc' or 'c' denote the wall shear stress calculated for uncontrolled/smooth cylinder and controlled cases, respectively.

The simulations were performed in cylindrical annuli at Re=4000. The various cases have been labelled in such a way that first two letters denote the Reynolds number and remaining denotes the SHS confugration, example 4kcg-4k denotes Re=4000 and cg denotes azimuthal or streamwise grooves, Also in $4k_g$cg the sub script 'g' denotes the case with enhanced η. Similarly ag,sp,posts denotes axial,spiral inclined at 20^o and posts SHS configurations, respectively. The statistics have been plotted as a function of wall-normal direction after averaging done in streamwise and spanwise directions along with time. On the SHS, the velocity slips are generated in both streamwise and spanwise directions. As a result, the turbulence statistics show the combined effects of both streamwise and spanwise slips.

The simulations have been run till statistically stationarity gets achieved as shown in Fig-4. Table-3 shows the response of various cases ran at Re=4000 and $\eta = 0.5$ in terms of streamwise velocity slip, slip-length , spanwise velocity slip and percentage drag reduction. The case 4kcg gives maximum drag reduction having maximum slip length in viscous units. A comparison has also been made with the results of Min & Kim (2004), as they modelled the SHS by using slip boundary conditions for the cases (a) and (b) in which they used equal slip lengths in streamwise and spanwise directions. The linear extrapolation shows our results conforming well with their results.

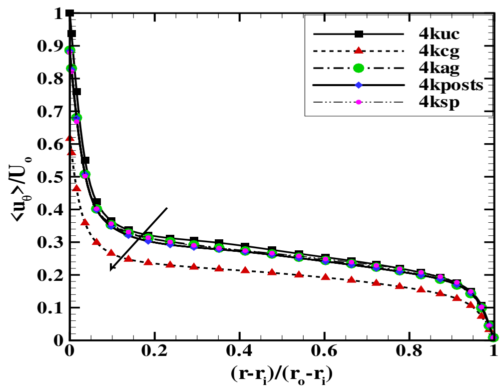

(a)

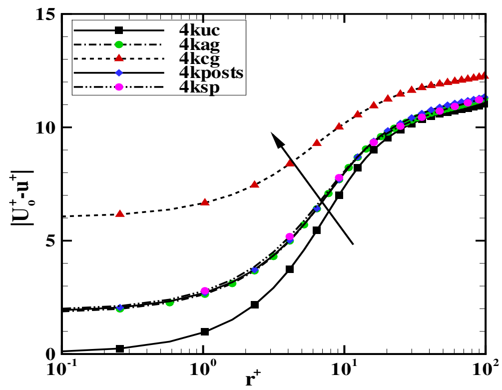

(b)

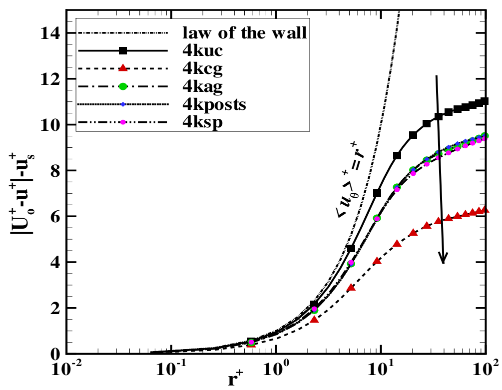

(c)

Figure 5. (a) Comparison of Mean streamwise velocity profiles along wall-normal direction among different SHS cases with a closer look at mean-velocity profiles: (b)$|U_o^+ - u^+|$; (c)$|U_o^+ - u^+| - u_s^+$ at Re=4000 and η =0.5.

3.1 Simulations with η= 0.5

Mean Flow

Fig-5(a) shows the wall normal variation of mean streamwise velocity for all the SHS cases. The different velocities at the inner wall are due to slip-velocities attained by various SHS cases according to their responses. The velocity at the inner wall represents the cumulative effect of no-slip and free-slip regions averaged over streamwise and spanwise directions with time. The downward arrow indicates increasing drag reduction with increasing velocity slip. Moreover, only no-slip region is responsible

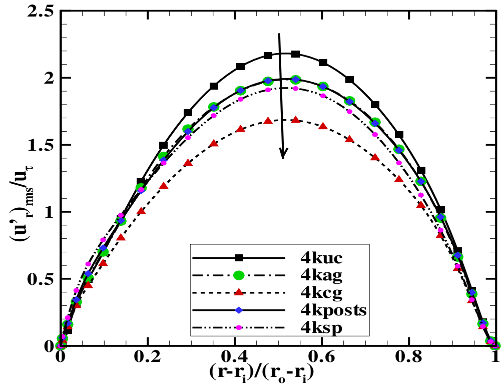

(a)

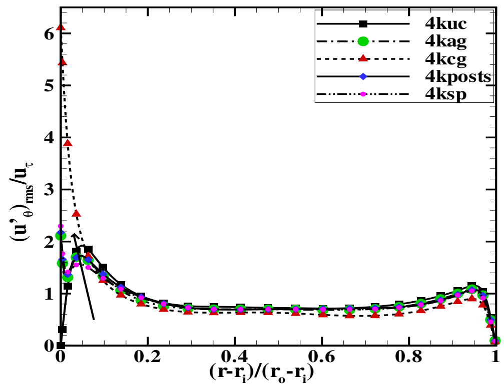

(b)

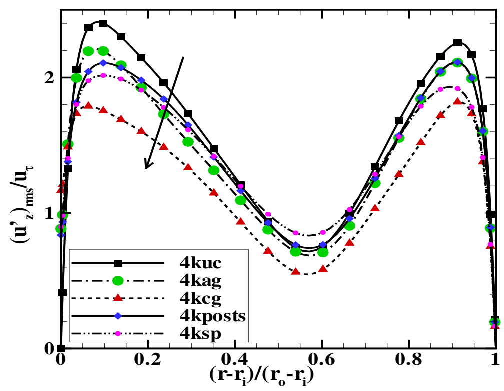

(c)

Figure 6. The rms velocity fluctuations normalized by u_τ : (a)wall-normal; (b)streamwise; (c)spanwise, at Re=4000 and $\eta = 0.5$.

for transferring angular momentum in the wall normal direction. Fig-5(b) and 5(c) shows the near-wall variation in viscous units (using uncontrolled case τ_{wall}). Fig-5(b) shows maximum slip velocity for case-4kcg at inner-wall while zero slip for 4kuc, with others showing intermediate slip. Upward arrow indicates increasing drag-reduction with increasing velocity slip. Fig-5(c) shows the velocity profiles collapsed in viscous sub-layer region onto the uncontrolled case. There is downward shift of profiles in buffer layer and log-law region with increasing drag reduction a feature similar to that in channel flows but unlike those cases(Min *et al.* (2003)andChoi *et al.* (1994)) which involve upward shift in log-law region .

Velocity Fluctuations

Fig-6 shows the variation of rms velocity fluctuations

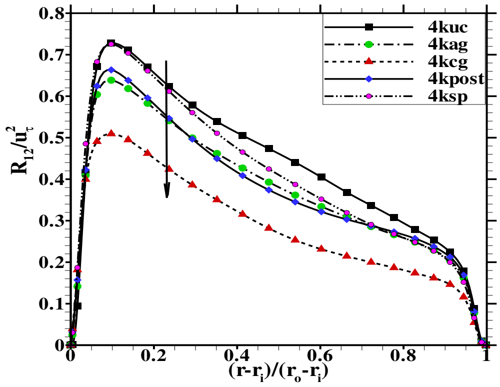

(a)

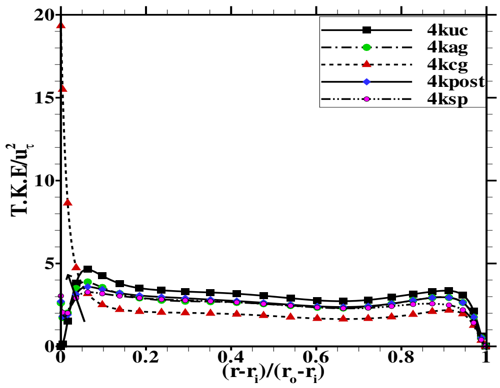

(b)

Figure 7. (a) Reynolds stress and (b) Turbulence kinetic energy profiles normalized by u_τ^2 at Re=4000 and $\eta = 0.5$.

in the wall-normal direction. The plots contain the contribution both from the turbulence and Taylor-vortices. Fig-6(a) shows the wall-normal velocity fluctuations with maxima in the mid-gap. There is downward shift of profiles with increasing drag reduction. Fig-6(b) shows that SHS has been able to modify the streamwise velocity fluctuations profiles in a small region near-wall, termed as "surface layer" by Rastegari & Akhavan (2015). Due to free-shear boundary condition, the values are non-zero for controlled cases at inner-wall. The streamwise SHS case-4kcg shows enhanced level of fluctuations near-wall due to inability of free-shear region to damp out the fluctuations. Also the increased fluctuations level is a sign of turbulence enhancement. Fig-6(c) apart from showing non-zero value of spanwise velocity fluctuations at inner-wall due to free-shear boundary condition there is decrease in levels with increasing drag reduction.

Reynolds stress & Turbulence Kinetic Energy

Fig-7(a) shows the wall-normal variation of Reynold's stress tensor component R_{12} where subscript 1 and 2 represent wall-normal and streamwise directions, respectively. Unlike channel flows it is positive throughout the wall normal direction. There is decrease in peaks near inner-wall with increasing drag reduction. Fig-7(b) shows enhanced level of production of TKE near inner-wall which is basically turbulence enhancement. While other controlled cases show finite values at inner-wall the case-4kcg shows maximum TKE.

Table 4. streamwise slip, spanwise slip & corresponding drag reduction at Re=4000 for η =0.5 & 0.67 .

Case	η	streamwise slip	spanwise slip	% DR
4kcg	0.5	0.3833	0.0146	31.3
4kag	0.5	0.1134	0.00466	10.84
4kposts	0.5	0.116	0.00212	9.64
4ksp	0.5	0.121	0.0023	7.3
4k$_g$cg	0.67	0.387	0.00061	31.4
4k$_g$ag	0.67	0.1499	0.00102	7.8
4k$_g$posts	0.67	0.1524	0.00088	10.8
4k$_g$sp	0.67	0.12	0.0059	-3.9

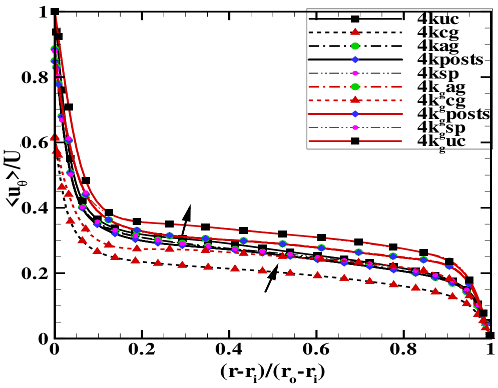

Figure 8. Comparison of Mean streamwise velocity profiles along radial direction among different SHS cases at Re=4000 with $\eta = 0.5(black)\&0.67(red)$.

3.2 Simulations with η= 0.67

In this section we have studied the effect of decreasing the annular gap on the Taylor-vortices, turbulence and their final effects on SHS performances. We are actually decreasing the characteristic gap width which is going to decrease the inertia effects bringing laminarizing effects into play due to decreasing the largest eddy size and its corresponding energy content.

Table-4 shows a comparison between the cases studied at η = 0.5 and 0.67 at Re=4000. We can see the case-"cg"(streamwise SHS) shows almost no change in either streamwise velocity slip and the corresponding %DR with enhanced η. The case-"ag"(axial SHS) shows a decrease of about 3% in %DR though there is considerable increase in streamwise slip. The case-"posts" show minor increase in drag reduction. It is the case-"sp"(spiral SHS) which show major change. The streamwise slip is nearly same but the spanwise slip has increased by almost 3 times which has resulted in drag enhancement upto 4% and change in drag of about 13% with increasing η.

Mean Flow

Fig-8 shows the comparison of streamwise velocity for controlled cases, specifically its wall-normal variation at η =0.5 and 0.67 . On the inner-wall apart from minor differences in slip velocity there is decrease in gradients with enhanced η. In the mid-gap, there is an upward shift in profiles due to enhanced transfer of angular momentum by Taylor-vortices in the wall-normal direction with reducing

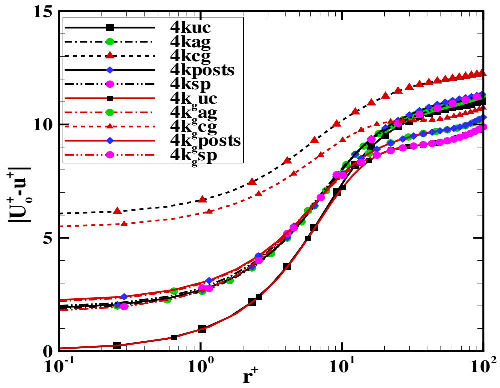

Figure 9. A closer look at mean streamwise velocity profiles: $|U_o^+ - u^+|$ at Re=4000,$\eta = 0.5$(black) & 0.67(red)

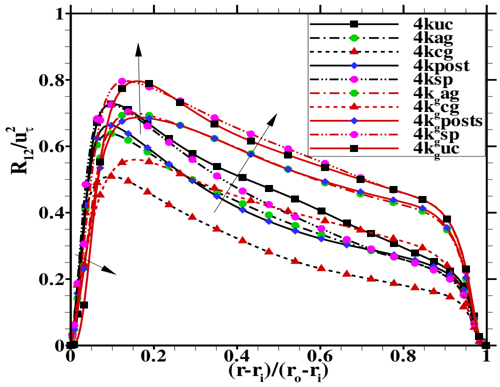

Figure 10. Reynolds stress profiles comparison for η =0.5(black) and 0.67(red) normalized by respective u_τ^2 at Re=4000.

gap width.

Fig-9 shows the comparison of near-wall variation of streamwise velocity in viscous units. On the inner wall most of the profiles overlap with their η =0.5 counterpart. The case-"cg" shows a decrease in absolute slip at the inner wall.

Reynolds stress

Fig-10 shows the comparison between R_{12} levels. With increase in η, the levels increase with maximum increase for case-4k$_g$uc and 4k$_g$sp thereby indicating increase in turbulence level and strength of Taylor-vortices. This increase in R_{12} might be the reason why for case-4k$_g$sp there is a drag increase of 4% as shown in Table-4.

Conclusion

We have studied turbulent drag-reduction in an incompressible Taylor-Couette flow by implementing SHS on inner rotating cylinder wall. Effect of different patterns of SHS along with increased radius ratio have been studied. SHS were modelled as idealized flat shear-free interfaces. Study was conducted for Re=4000 based on gap width. We were able to achieve maximum drag-reduction upto 31%, which occured for the streamwise SHS. The enhanced η hardly affects DR except for spiral SHS, where it brings about an increase in drag. The SHS implementation results in enhanced production of TKE, which is basically turbulence enhancement yet we observe drag reduction for most cases implying that slip is the major contributor towards drag reduction.

Acknowledgements
The authors would like to thank the Computational Fluid Dynamics & High Performance Computing Lab's staff for support.

REFERENCES

Ahmad, H, Baig, MF & Fuaad, PA 2015 Numerical investigation of turbulent-drag reduction induced by active control of streamwise travelling waves of wall-normal velocity. *European Journal of Mechanics-B/Fluids* **49**, 250–263.

Cheng, Liang & Armfield, Steven 1995 A simplified marker and cell method for unsteady flows on non-staggered grids. *International journal for numerical methods in fluids* **21** (1), 15–34.

Choi, Haecheon, Moin, Parviz & Kim, John 1994 Active turbulence control for drag reduction in wall-bounded flows. *Journal of Fluid Mechanics* **262**, 75–110.

Dong, S 2007 Direct numerical simulation of turbulent taylor–couette flow. *Journal of Fluid Mechanics* **587**, 373–393.

Fuaad, PA, Baig, MF & Ahmad, H 2016*a* Drag-reduction in buoyant and neutrally-buoyant turbulent flows over super-hydrophobic surfaces in transverse orientation. *International Journal of Heat and Mass Transfer* **93**, 1020–1033.

Fuaad, PA, Baig, MF & Khan, BA 2016*b* Turbulent drag reduction using active control of buoyancy forces. *International Journal of Heat and Fluid Flow* **61**, 585–598.

Khan, BA & Baig, MF 2016 Turbulent drag reduction in channel flow using weak-pressure forcing. In *Advances in Computation, Modeling and Control of Transitional and Turbulent Flows*, pp. 195–203. World Scientific.

Kuwahara, Kunio 1999 Unsteady flow simulation and its visualization. In *30th Fluid Dynamics Conference*, p. 3405.

Lee, Choongyeop & Kim, Chang-Jin 2011 Underwater restoration and retention of gases on superhydrophobic surfaces for drag reduction. *Physical review letters* **106** (1), 014502.

Min, Taegee & Kim, John 2004 Effects of hydrophobic surface on skin-friction drag. *Physics of Fluids* **16** (7), L55–L58.

Min, Taegee, Yoo, Jung Yul, Choi, Haecheon & Joseph, Daniel D 2003 Drag reduction by polymer additives in a turbulent channel flow. *Journal of Fluid Mechanics* **486**, 213–238.

Ou, Jia, Perot, Blair & Rothstein, Jonathan P 2004 Laminar drag reduction in microchannels using ultrahydrophobic surfaces. *Physics of fluids* **16** (12), 4635–4643.

Park, Hyungmin, Sun, Guangyi *et al.* 2014 Superhydrophobic turbulent drag reduction as a function of surface grating parameters. *Journal of Fluid Mechanics* **747**, 722–734.

Rastegari, Amirreza & Akhavan, Rayhaneh 2015 On the mechanism of turbulent drag reduction with superhydrophobic surfaces. *Journal of Fluid Mechanics* **773**.

Rosenberg, Brian J, Van Buren, Tyler, Fu, Matthew K & Smits, Alexander J 2016 Turbulent drag reduction over air-and liquid-impregnated surfaces. *Physics of Fluids* **28** (1), 015103.

Srinivasan, Siddarth, Choi, Wonjae, Park, Kyoo-Chul, Chhatre, Shreerang S, Cohen, Robert E & McKinley, Gareth H 2013 Drag reduction for viscous laminar flow on spray-coated non-wetting surfaces. *Soft Matter* **9** (24), 5691–5702.

Van Buren, Tyler & Smits, Alexander J 2017 Substantial drag reduction in turbulent flow using liquid-infused surfaces. *Journal of Fluid Mechanics* **827**, 448–456.